



SEWING

IST-2000-28084

System for European Water monitorING

Deliverable 12:

Optimisation and parameter extraction software

Version: 1st
Report Preparation Date: 25 June 2003
Classification: FP5 use only
Contract Start Date: 01.09.2001
Duration: 36 months
Project Co-ordinator: Politechnika Warszawska, Poland
Partners: Politechnika Warszawska - PL, Instytut Technologii Elektronowej - PL., Technical University of Lodz - PL., Valtion Teknillinen Tutkimuskeskus - FI, Centre National de la Recherche Scientifique - F, MICROSENS - CH, Universitat Politecnica Catalunya - E, Institut fuer Wasserversorge, Gewaesserekologie und Abfallwirtschaft - A, SYSTEVA- I.



**Project funded by the European Community
under the “Information Society Technology”
Programme (1998-2002)**

Project Number: IST-2000-28084
Project Acronym: SEWING
Title: System for European Water monitorING

Deliverable N°: 12. Optimisation and parameter extraction software
Due date: 30.06.2003
Delivery Date: 25.06.2003

Short Description:

Deliverable 12: Optimisation and parameter extraction software

Deliverable No 12 is based on the research results previously presented in Deliverables 10 and 11 (behavioural and physical modelling of ISFET and CHEMFET sensors) as well as on the data on the physical properties of the sensors provided by the manufacturers and given in the previous deliverables.

The sensor measurements were carried out both for sensors manufactured at IET and LAAS. In case of the sensors from IET the measurements were performed on the dedicated measurement stand at WUT. In the case of the sensors from LAAS a separate measurement stand was designed so as to investigate their sensitivity as well as electrical properties. The measurement results are presented in this deliverable.

The measurements enabled verification of the developed physical and behavioural models. Some improvements to the existing models were introduced so as to attain better agreement between the measurements and the simulation results.

For the accurate sensor characterization purposes, the specialized software was developed. For H⁺ sensitive ISFET it was implemented in MINUIT and MATLAB environments. Owing to the developed software, efficient parameter extraction and identification was possible.

As a result the set of important parameters characterizing the sensors were obtained. Results of optimisation and parameter extraction are presented and the fitting error is calculated.

In the case of CHEMFET sensors its physical model has been optimised, its electrical part has been modified to improve accuracy, possibilities of identification. Temperature dependencies of parameters were introduced and the model was tested. Procedures for pre-extraction and extraction of the model parameters have been introduced.

Moreover generalized versions of models, taking into account different electrovalencies of ions and anit-ions have been developed. The physical model of Van den Berg and the explicit SNE model of Ogrodzki have been extended. Final model has been implemented in SPICE, SPECTRE and OPTIMA environments.

A problem of relations between chemical parameters and the sensor operating point has been investigated and the model was optimised.

Also variability of the model parameters was explored and presented.

Partners owning: Politechnika Łódzka, Politechnika Warszawska

Partners contributed: LAAS-CNRS, UPC

Made available to: Mr. Mario Verdese, Project Officer.

I - Introduction

Two ISFET realizations previously accepted for the SEWING objectives were taken into account (IET, LAAS). The mentioned sensors were described through the models presented in previous deliverables (10 and 11) where both behavioral and physical models for CHEMFET were presented. Next, the measurements were performed so as to render possible the characterization of the devices. The dedicated software was developed in order to provide parameter extraction from the measurements for the developed models. The measurements were performed both at WUT and TUL DMCS. The dedicated software was developed with application of MINUIT and MATLAB environments.

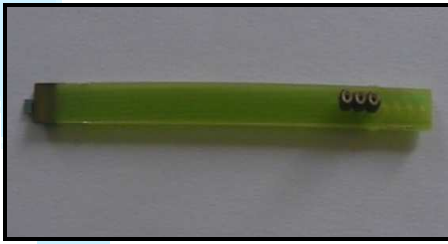


Figure 1.1. ISFET from LAAS

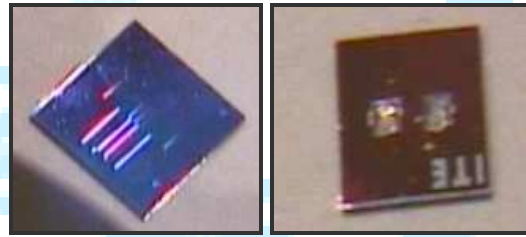


Figure 1.2. ISFET from IET. Front side (left), back side of the wafer (right)

The CHEMFET sensor models have been optimised, essential improvement of its electrical part optimised its accuracy and possibilities of parameters identification. Especially temperature dependencies have been introduced. Parameters identification requires rough pre-extraction followed by optimisation based exact mini-max or least squares approaches. A problem of relations between chemical parameters and the sensor operating point was also investigated and the model enabled optimal selection of the operating point. Also variability of the model parameters was explored and presented in this work.

So far introduced models have been generalized, taking into account possible different electrovalencies of ions. The physical model of Van den Berg and the explicit SNE model of Ogrodzki have been extended to take into account so general case. Models are implemented in SPICE (Windows), SPECTRE (SUN Workstations) and OPTIMA (DOS) environments.

2. Optimization of models for their best use for circuit simulation

2.1.1. Improvement of the chemical part of the model

The existing models of ISFET were describing the ideal (Nernstian) response of the chemosensorial curve (deliverable 10, deliverable 11). The “Nernstian” sensitivity was estimated at a level of $\approx 60\text{mV/pH}$. However, measurements revealed that the sensitivity of real sensors could slightly differ from the ideal behavior (for example measured sensitivity of the sensor manufactured by LAAS was around 53mV/pH). In order to account for this phenomenon the fitting coefficients were introduced to the existing models. This lowered the modeled sensitivity and made it more realistic. These models were presented in the previous deliverables. The fitting coefficients were the object of parameter extraction.

2.1.2. Improvement of the semiconductor part of the model

The first attempt on the way to characterize the semiconductor part of the ISFET was to apply the Schichman–Hodges model of MOSFET known as SPICE LEVEL 1. However it occurred, that the fitting of the measurements implementing this model produced unsatisfying results. This was the reason to introduce some modifications concerning in particular the carrier mobility degradation in the channel of the transistor. The fact that the transistor under consideration was wide and long allowed the simplification of the model by neglecting most of the short channel terms. Finally modified SPICE LEVEL 3 model was adopted. It is represented by the following equations.

For either linear and saturation region the following formula takes effect:

$$I_D = \frac{C_{ox} \mu_{eff} W_{eff}}{2 L_{eff}} (2(V_{GS} - V_T^{ISFET}) - V_{DS}) V_{DS}$$

the carrier mobility is modified by the vertical and perpendicular field in the channel:

$$\mu_{eff} = \frac{\mu_s}{1 + \mu_s \frac{V_{DS}}{v_{max} L}} \quad \mu_s = \frac{\mu_0}{1 + \theta (U_{GS} - V_T^{ISFET})}$$

When the transistor is operating in the saturation region, the actual drain voltage V_{DS} must be substituted by the saturation drain voltage V_{DSsat} . The saturation voltage of an ISFET can be expressed as:

$$V_{DSsat} = V_{GS} - V_T^{ISFET} + v_{max} \frac{L_{eff}}{\mu_{eff}} - \sqrt{(V_{GS} - V_T^{ISFET})^2 + \left(v_{max} \frac{L_{eff}}{\mu_{eff}} \right)^2}$$

with the modified threshold voltage as below:

$$V_T^{ISFET} = V_T^{MOS} - \Psi_s - \Phi_m + const$$

In Figure 2.1.the comparison of the model LEVEL 1 with LEVEL 3 is presented. The solid lines correspond to the fitted characteristics for the improved model. The dashed lines represent the fitting results for the original simple SPICE Level 1 model. The circles denote the average measured values for the six properly working transistors. As it can be seen the modified MOS model SPICE LEVEL 3 fits much better the measured curves.

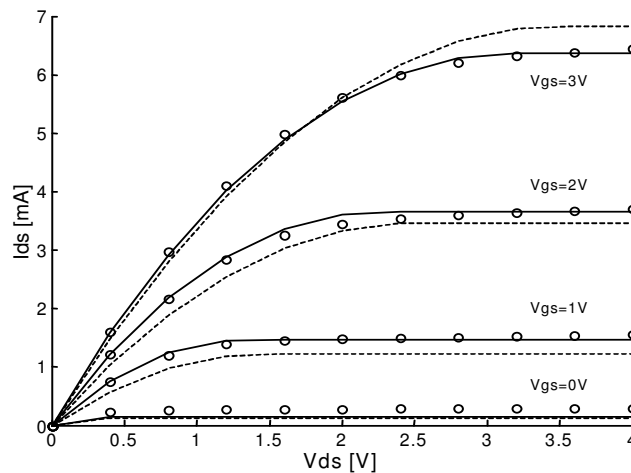


Figure 2.1. Comparison of MOS MODEL SPICE LEVEL 1 (dashed) to MOS MODEL SPICE LEVEL 3 (solid) and measurements (dots)

2.1.3 Temperature influence modeling

The measurements demonstrate that temperature influences significantly both semiconductor and chemical part of the sensor, which cannot be neglected in the model. The main parameters responsible for the thermal dependence were extracted. From the point of view of the model, the following temperature dependent formulas were implemented:

- a) changes of the dissociation constants $K_x(T) = K_x(300)^{300/T}$
- b) changes of the reference electrode potential $E_{ref} = E_0 + E(T)(T - 300)$
- c) changes of the “active potential” on the border of phases
- d) changes of the carrier mobility

$$\mu_{eff} = \frac{\mu_s}{1 + \mu_s \frac{V_{DS}}{V_{max} L}} \left(\frac{T}{300} \right)^{-a}; \quad \mu_s = \frac{\mu_0}{1 + \theta(U_{GS} - V_T)}; \quad (a \approx 1.5)$$

- e) changes of the threshold voltage resulting from the temperature influence on the Fermi level, the energy bandgap in silicon as well as the intrinsic carrier concentration

$$n_i(T) = B \left(\frac{T}{T_0} \right)^{\frac{3}{2}} \exp\left(-\frac{W_g}{2kT}\right) \quad W_g(T) = W_g(0) - \frac{\alpha T^2}{\gamma + T}$$

$$V_T^{ISFET}(T) = V_T^{MOS}(T) - \Psi_s(T) - \Phi_m + const$$

2.2 CHEMFET models development and improvement (PW)

2.2.1. Improvement of electrical model

To reduce influence of the internal MOSFET properties upon the CHEMFET sensor response typically the operating point (U_{DS} and ID) is fixed by a biasing circuitry of the sensor. For such a mode of operation the CHEMFET device can be represented by the chemo-electrical model where the chemical part is not dependent on the electrical part, so the MOSFET device can be viewed as separable from the chemo-electrical transducer, where the ionic activity is converted into V_{GR} according to models described in III.1 or III.2.

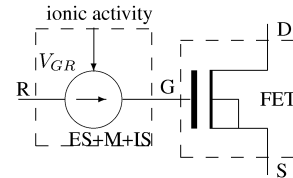


Figure. 2.2. Separable CHEMFET model

We have been dealing solely with CHEMFETs built upon FET structures manufactured at IET. Depletion type FETs require more involved modelling – in comparison to more common enhancement devices. As a compromise between simplicity and accuracy, a depletion MOSFET model described by Merckel was adapted (see deliverable 10 and [ICSES02-LJO]). It contains 7 parameters as listed in the Table. For use as a separable CHEMFET model one should replace U_{GS} with $URS + V_{GR}$, where URS is the reference electrode-source voltage and V_{GR} models the transducer activity. Recently smoothness of the model has been improved [MIXDES03-LJO] in the saturation region. Let us denote:

$$U_{GP} = U_{GS} - V_{OFF}, \quad U_{GF} = U_{GS} - V_{FB},$$

$$V_{DSS1} = V_E \left(\sqrt{1 + \frac{2U_{GS} - V_{OFF}}{V_E(1 + \delta)}} - 1 \right), \quad V_{DSS2} = V_E \left[\sqrt{1 + \frac{2}{1 + \delta} \cdot \left[\frac{U_{GP}}{V_E} - \frac{r-1}{2} \left(\frac{U_{GF}}{V_E} \right)^2 \right]} - 1 \right],$$

$$V_{DSS3} = V_E \left[\sqrt{1 + \frac{2}{r + \delta} \cdot \frac{U_{GP} + (r-1)U_{GF}}{V_E}} - 1 \right], \quad r = \frac{r_0}{1 + \theta \cdot U_{GF}}$$

The model distinguishes 3 ranges of U_{GS} voltage:

1. For $U_{GS} < V_{OFF}$: $I_D = 0$
2. For $V_{OFF} \leq U_{GS} \leq V_{FB}$ - depletion region.
 - (a) If $U_{DS} \leq V_{DSS1}$ (linear), then $I_D = \beta \cdot \left(U_{GS} - V_{OFF} - U_{DS} \frac{1 + \delta}{2} \right) \cdot U_{DS}$
 - (b) Otherwise (saturation region): $I_D = I_{DSS1} \cdot \left(1 + \frac{U_{DS} - V_{DSS1}}{V_E + V_{DSS1}} \right)$, where I_{DSS1} is calculated from (2a) for $U_{DS} = V_{DSS1}$.
3. If $U_{GS} \geq V_{FB}$ and $U_{GS} - V_{FB} \geq U_{DS} \geq 0$ (fully enhanced):
 - (a) If $U_{GF} \leq U_{DS}$, then:
 - if $U_{DS} \leq V_{DSS2}$ then $I_D = \beta \cdot \left(\left(U_{GP} - U_{DS} \frac{1 + \delta}{2} \right) \cdot U_{DS} + (r-1) \frac{U_{GF}^2}{2} \right)$
 - else $I_D = I_{DSS2} \left(1 + \frac{U_{DS} - V_{DSS2}}{V_E + V_{DSS2}} \right)$, where I_{DSS2} calculated as above for $U_{DS} = V_{DSS2}$
 - (b) else $I_D = \beta \cdot \left[\left(U_{GP} - U_{DS} \frac{1 + \delta}{2} \right) + (r-1) \cdot \left(U_{GF} - \frac{U_{DS}}{2} \right) \right] \cdot U_{DS}$.
4. If $U_{GS} \geq V_{FB}$ and $U_{GF} > V_{DSS3}$, then (partly enhanced).
 - (a) If $U_{DS} \leq V_{DSS3}$ (linear):
$$I_D = \beta \cdot \left[\left(U_{GP} - U_{DS} \frac{1 + \delta}{2} \right) + (r-1) \cdot \left(U_{GF} - \frac{U_{DS}}{2} \right) \right] \cdot U_{DS}$$
 - (b) otherwise (saturation): $I_D = I_{DSS3} \left(1 + \frac{U_{DS} - V_{DSS3}}{V_E + V_{DSS3}} \right)$, I_{DSS3} calculated from (4a) for $U_{DS} = V_{DSS3}$

Table 2.1. Electrical parameters of the CHEMFET sensor

Parameter	Name	Typical value
β	Transconductance	1.26 [mS/V]
V_{OFF}	Offset voltage	-2.28 [V]
V_{FB}	Flat bands voltage	-0.215 [V]
V_E	Early voltage	32.7 [V]
δ		0.181
θ		$2.92 \cdot 10^{-3}$ [V^{-1}]
r_0		1.4
α	Mobility related exponent	-1.5
dThdT	Temp. sensitivity of θ	
dr0dT	Temp. sensitivity of r_0	
dV0dT	Temp. sensitivity of V_{OFF}	
t_{nom}	Reference temperature	20C

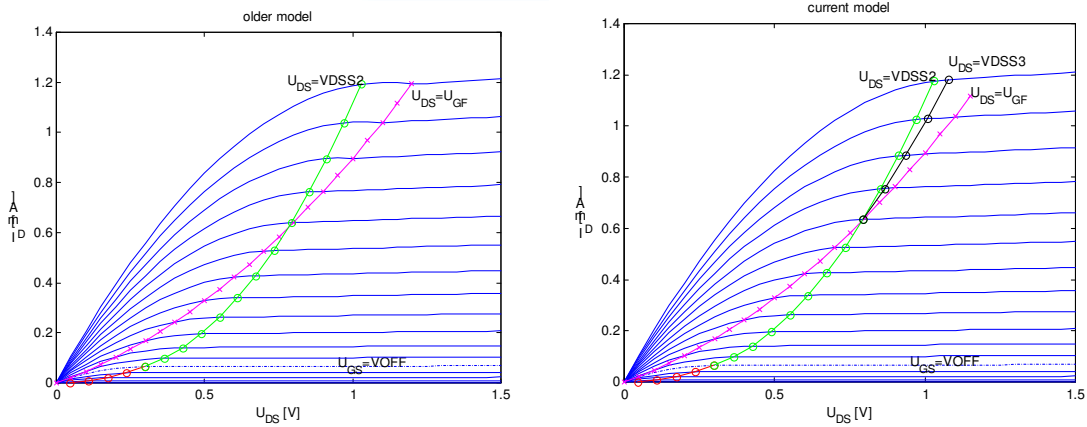


Figure 2.3. Geometrical explanation of the Merckel model modification

As seen from the above figures for larger U_{GS} biasing switching from linear to saturation mode in the older model took place along $U_{DS}=U_{GF}$ line. In the current model the switching takes place along $U_{DS}=VDSS3$ line, which results in smooth transition of the drain current as well as its derivative dI_D/dU_{DS} .

2.2.2. Temperature dependence of model parameters

To reduce influence of internal FET properties upon CHEMFET sensor characteristics - the measurement circuit typically keeps the operating point of the FET, i.e. its drain current I_D and the drain to source voltage U_{DS} , constant. For fixed temperature constant values of I_D and U_{DS} induce constant value of the insulator surface to source voltage U_{GS} . Consequently the changes of the measurable reference electrode to source voltage $U_{RS} = U_{GS} - U_{GR}$ can be attributed solely to changes of the chemically influenced voltage U_{GR} . One way of handling the situation is modelling of the temperature dependence of the insulator surface to source voltage U_{GS} . Since U_{GS} is not measurable directly – we have been modelling joint effects of temperature on the FET (U_{GR}), membrane and electrolytes (U_{GR}), using U_{RS} values from measurements to determine model parameter values.

For the sensors delivered by IET it turned out that the following temperature dependencies of FET model parameters made the CHEMFET reasonably accurate:

$$\begin{aligned} \beta(T) &= \beta \cdot \left(\frac{T}{T_{nom}} \right)^\alpha, & T_{nom} &= t_{nom} + 273.15 \\ V_{OFF}(T) &= V_{OFF} \cdot (1 + dV_{OFF}/dT \cdot (T - T_{nom})) \\ r_0(T) &= r_0 \cdot (1 + dr_0/dT \cdot (T - T_{nom})) \\ \theta(T) &= \theta \cdot (1 + d\theta/dT \cdot (T - T_{nom})) \end{aligned}$$

An example of fitting a NO₃ sensitive CHEMFET measurement data (t=10,20,30C) resulted in maximum relative error: 6.3% and mean square error: 3.6%. See also the plots of the measurement data and model predictions for different ionic activities.

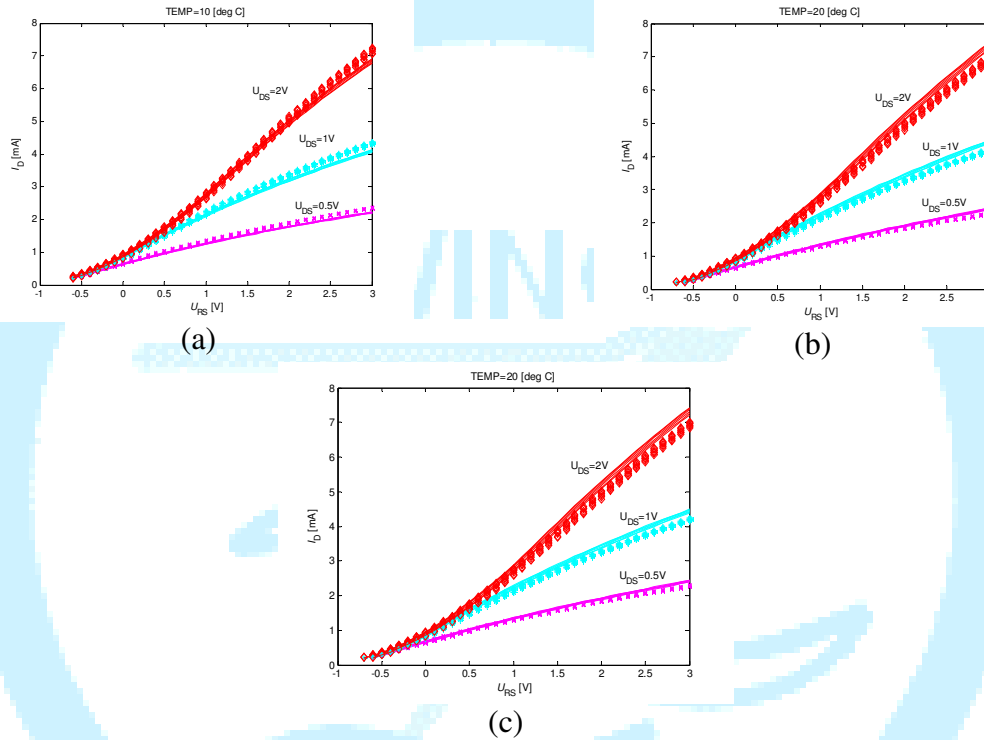


Fig. 2.4. Transfer characteristics of a fitted CHEMFET sensor at (a) 10C (b) 20C (c) 30C: measured (markers) vs model (solid lines).

Similar temperature relations hold for the chemical interface, where temperature influences its voltage offset and selectivity:

$$V_{Moff}(T) = V_{Moff}(T_0) - \psi_0 \ln(a_{1R}) (T - T_0) / T_0$$

$$K_j(T) = K_j(T_0) + dK_j dT (T - T_0)$$

These parameters are explained in p.2.2.4.

It is expected that measurements of the industrial grade sensors (their availability has been postponed due to some technological problems) will make it possible to tune the thermal dependencies of our model even better.

2.2.3. Operating point influence on sensor responses

Dependence of CHEMFET sensor on biasing can be seen from measurement in Fig. 2.5.

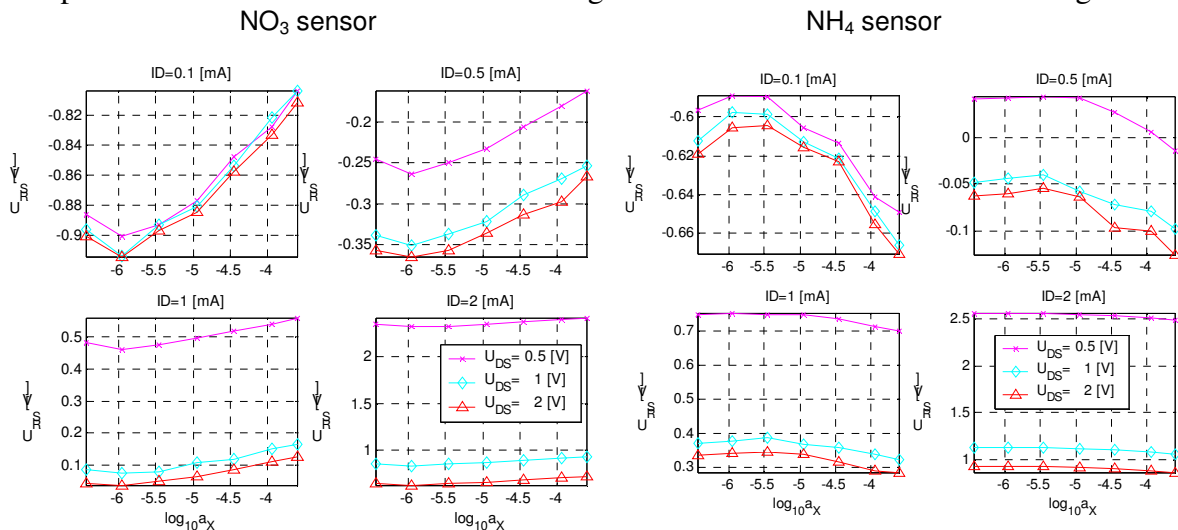


Figure 2.5. Dependence of sensor responses on operating point for a NO_3 and a NH_4 sensor

For rational design of the CHEMFET sensor it was necessary to develop a CHEMFET model which does not assume any biasing – so it can be used for design of biasing circuitry. Besides the model should include a subtle dependency of sensor response V_{GR} not only on ions but also on the operating point I_D , V_{DS} (see [MIXDES02-LJO] for details). Separable models cannot adequately reflect this interaction between the chemical and electrical part. For the above presented depletion FET model the situation is illustrated with Fig. 2.6 – to the left.

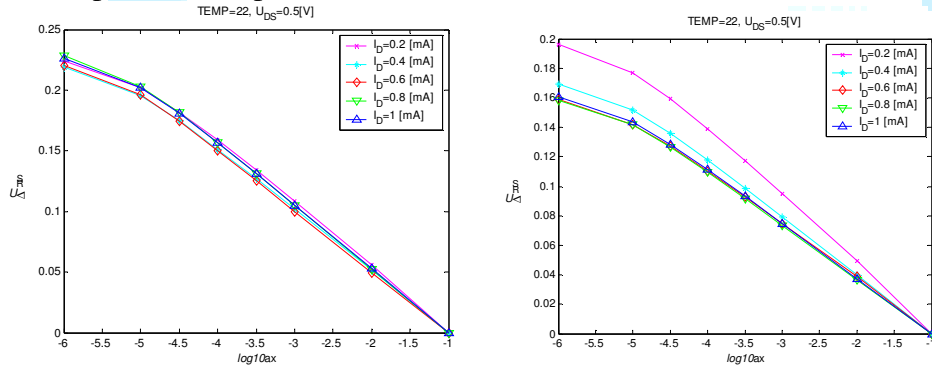


Figure 2.6. Responses of a model with no dependence on the operating point (left) and of the proposed model (right)

Change of the drain current shifts the sensor response only. It turned out that proper dependence of sensor response on the operating point can be modelled by restricting influence of the ion-dependent V_{GR} voltage to the cut-off voltage V_{OFF} of the model. Replacement of $U_{GS}=U_{RS}+U_{GR}$ with $V_{OFF} \leq V_{OFF}-U_{GR}$ produces sensor characteristics (Fig. 2.6– to the right) with desirable dependency on the operating point ([MIXDES02-LJO]).

We would like to investigate some unexpected phenomena which occur at relatively large drain-source biasing (i.e. in the region that has been disregarded for practical use – because of power consumption). It can be seen in the Figure 2.7, that chemical sensitivity of the drain current is much larger in this region then anywhere else. It remains to be seen if this effect is sufficiently stable and predictable, so it can be used for sensing.

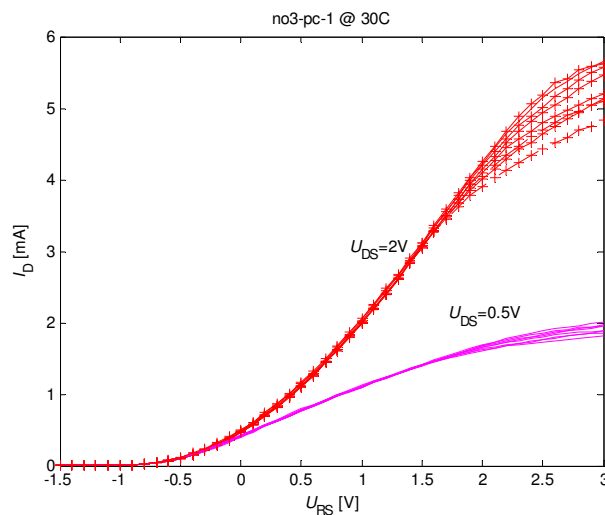


Figure 2.7. Transfer I-V curves for a NO₃ sensing CHEMFET

2.2.4. Analysis of numerical properties of models

Efficiency and accuracy of an identification task for the CHEMFET membrane model are strongly dependent on numerical properties of the task. Two essential numerical problems have been solved: a) transformation of a set of primary, physical model parameters into a set of independent, secondary parameters, providing a non-ambiguous identification task, b) analysis of sensor response sensitivity to the secondary parameters.

The following primary, technological parameters are known from physical modeling of phenomena in the ion-selective membrane: n_i - nonideality index, k_{Cj} - division constants for ions, β_j - complexation constants for ions, K_{aj} - association constants for ions, \bar{a}_{Ltot} - total concentration of a ionophore, \bar{a}_{Ytot} - total concentration of a lipophylic salt, k_{Ai} - division constants for anti-ions, a_{C1R} - main ions activity in the reference solution, E_{FET} - FET offset voltage. However identification of most of these parameters is an ill-conditioned task. Several possibilities of variables transformation have been checked and a transformation into the following set of secondary parameters has been finally chosen: n_i - nonideality index,

$K_j = \frac{\beta_j k_{Cj}}{\beta_1 k_{C1}}$ - intrinsic selectivity, $E_{offs} = E_{FET} + \psi_0 \ln a_{C1R}$ - intrinsic offset voltage, K_{aj} - association constants for ions, \bar{a}_{Ltot} - ionophore concentration, \bar{a}_{Ytot} - lipophylic salt concentration, $k_{Ai} k_{C1} \beta_1$ - normalized division constants for anti-ions, $k_{Ci} / k_{C1} \beta_1$ - normalized division constants for cations, $1/\beta_j$ - inverts of complexation constants. In the above parameters index 1 denotes a main ion for the device.

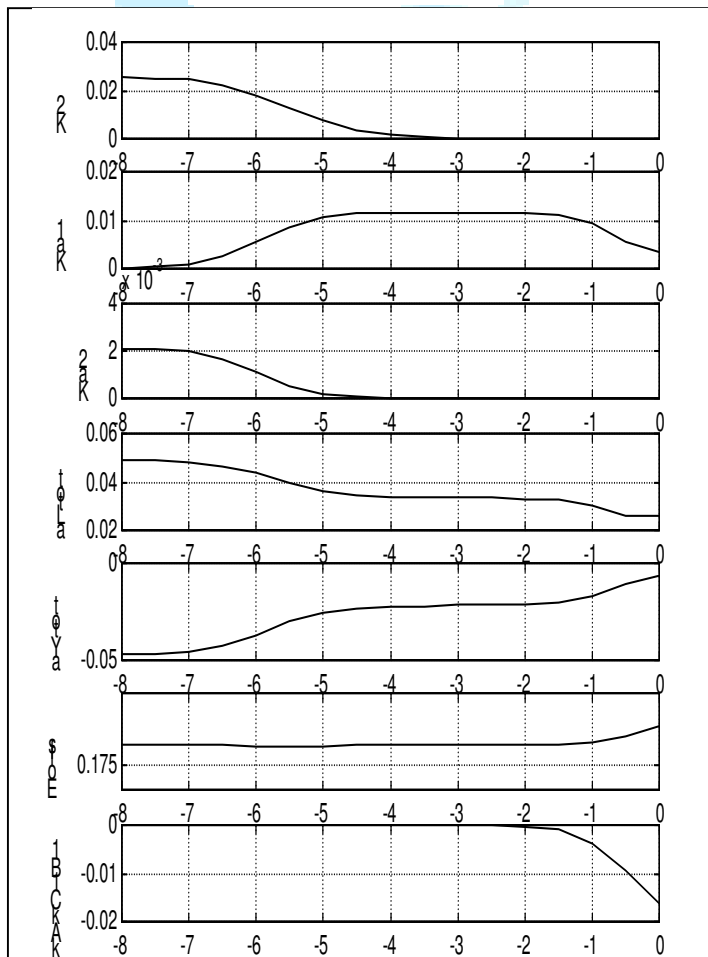


Fig. 2.7. Semirelative sensitivities of a CHEMFET response with respect to secondary parameters

To test identificability of the model semirelative sensitivities of the sensor response with respect to secondary parameters have been calculated as functions of main ions concentration. We observe that essential for identification are the most influencing parameters: E_{offs} (sensitivity: $\sim 10^{-1}$), K_j , \bar{a}_{Ltot} , \bar{a}_{Ytot} , K_{a1} (sensitivity: $\sim 10^{-2}$). Weakly identifiable is K_{a2} (sensitivity: $\sim 10^{-8}$) influencing only the small concentration region. Anti-ion dependent parameter $k_{Ai} k_{C1} \beta_1$ influence a high concentration knee, not observable in good quality sensors, and hence it might be identified only from high concentration measures (sensitivity: $\sim 10^{-2}$ in the high concentration region). Influence of parameters $k_{Ci} / k_{C1} \beta_1$ and $1/\beta_j$ is negligible and so their identification is

impossible in practice.

2.2.5. Generalization of the Super-Nikolski model

In Deliverable 10 a super-Nikolski model of CHEMFET sensors has been developed for the case of identical electrovalencies of all ions of the same sign. In general we have an electrolyte containing ions of the same sign, but different electrovalencies: $z_0, z_1, z_2, \dots, z_n$, i.e. positive for a cations sensitive sensors and negative for an anions sensitive one. Electrovalency of lipophylic salt anti-ions is of an opposite sign, and we denote it by $-z_Y$, i.e. z_Y is also positive for the cations sensitive sensor and negative for the anions sensitive one. Thus the ratio z_j / z_Y is always positive. The super-Nikolski model neglects influence of anions and cations in the charge balance, since dominating are charged complexes in the ionophore (containing ligands or lipophylic salt anti-ions). Thus the general Van den Berg equation introduced in Deliverable 10 reduces to the form:

$$\frac{-\bar{\alpha}_{LY}C_1}{1+C_1} + \frac{(C_1+1)}{1+C_3} = 0$$

where $C_1 = a_0 e_B^{z_0} + \sum_{j=1}^m K_j a_j e_B^{z_j}$, $C_2 = k_{a0} a_0 e_B^{z_0} + \sum_{j=1}^m k_{aj} K_j a_j e_B^{z_j}$, $C_3 = C_1 + C_2 a_{Ltot}$,

$C_{1w} = z_0 a_0 e_B^{z_0} + \sum_{j=1}^m z_j K_j a_j e_B^{z_j}$, $e_B = \exp \frac{-E_B}{\psi_0}$, $\psi_0 = nkT/q$, E_B is a membrane potential, a_j - the j th ion activity, $\alpha_{LY} = \frac{\bar{z} a_{Ltot}}{z_Y a_{Ytot}}$. In the above $\bar{z} = C_{1w} / C_1$, $\bar{K}_a = C_2 / C_1$

respectively mean a weighted average electrovalency and a weighted average lipophylic constant.

This gives a super-Nikolski-Eisenmann polynomial equation, called the SNE equation, of the order $\max(z_0, \dots, z_m)$

$$C_1 - \frac{1}{w} = 0$$

where $w = \frac{\alpha_{LY}}{2} \left(1 + \sqrt{1 + \frac{4z_Y a_{Ytot} \bar{K}_a}{\bar{z}}} \right) - 1$. If all electrovalencies are identical, not necessarily 1, then the model takes the form

$$E_B = \frac{1}{z_0} \psi_0 \ln \left[w \left(a_0 + \sum_{i=1}^m K_i a_i \right) \right]$$

Otherwise the polynomial equation has to be solved. If all ions are of valency 1 or 2 the SNE equation is quadratic and can be easily solved with respect to e_B . If $\max(z_0, \dots, z_m) = 3$ then the known analytical solution can also be introduced. Otherwise only approximate or numerical solutions of the SNE equation may be applicable.

3. Methods of model parameter extraction from measurement data

3.1. ISFET models identification

3.1.1. Software dedicated for parameter extraction

The measurements of the existing realization of the ISFET sensors were carried out. The sensors manufactured by IET were measured at WUT on a dedicated measurement stand. Measurements of the sensors from LAAS were performed at TUL DMCS on a dedicated measurement stand. The schematic representation of the stand is presented in Figure 3.1. The operating circuit of ISFET was connected with data acquisition board and PC. The acquisition process was controlled by the application developed in the LabVIEW environment. It allowed efficient data acquisition. Performed measurement constituted the base for further model verification and parameter extraction.

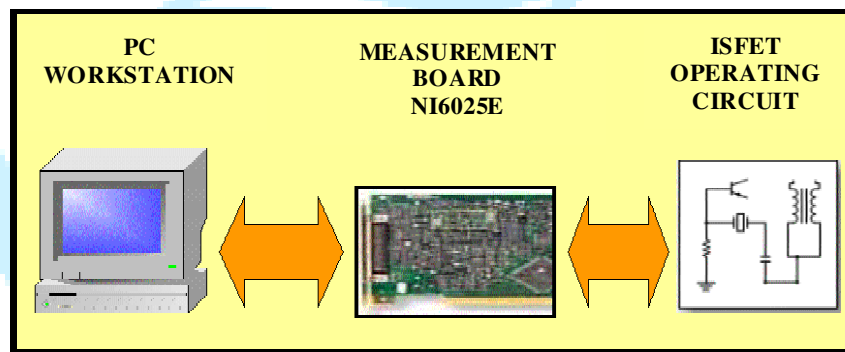


Figure 3.1. Schematic representation of the measurement stand at TUL DMCS

3.1.2 Measurements of the sensors

3.1.2.1 Measurement of LAAS sensors

The transistor possesses a channel 800 μm wide and 30 μm long. It is manufactured by LAAS (Toulouse). The set of 6 transistors was tested. Some the most important curves were presented in Figure 3.2–Figure 3.4. All of them showed good repeatability of output curves. The measured sensitivity was around 53mV/pH in the wide range of pH from 1 to 10. However after some time of tests three of them began to work improperly and had to be removed from the further measurements (probably for the reason of the loss of passivation tightness).

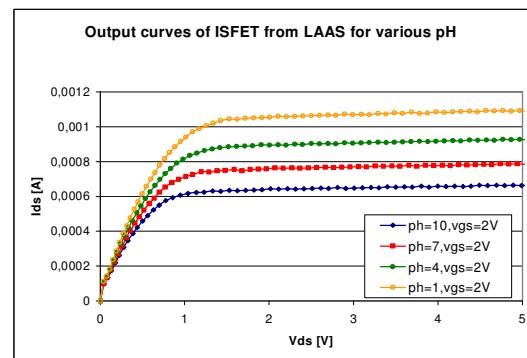
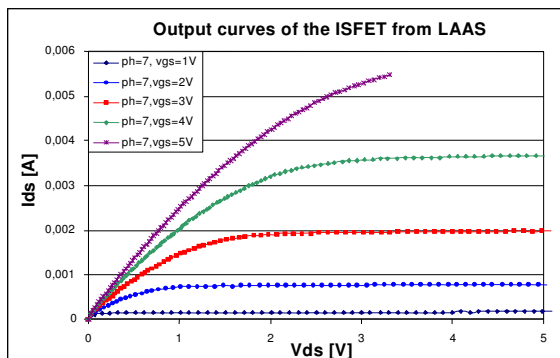


Figure 3.2. Measured output characteristics of the sensor from LAAS

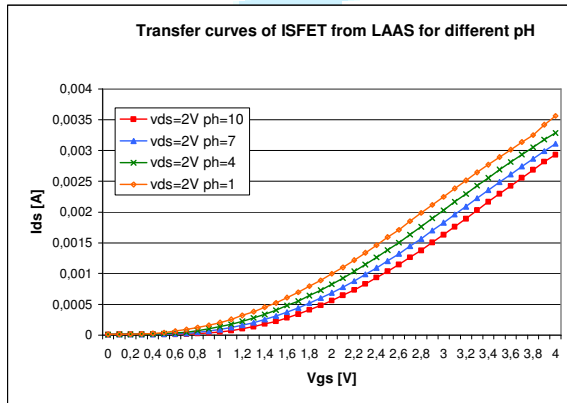


Figure 3.4a. Measured transfer curves of the sensor from LAAS for different pH values

Figure 3.3. Measured output characteristics of the sensor from LAAS for various pH values

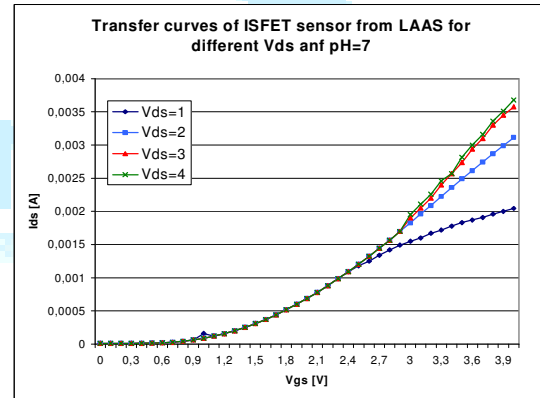


Figure 3.4b. Measured transfer curves of the sensor from LAAS for pH=7

3.1.2.2 Measurements of IET sensors

The important curves were presented in Figure 3.5–Figure 3.8. The measured ISFETs were manufactured at the Institute of Electron Technology in Warsaw, Poland. The transistors possess a built-in channel 640 μm wide and 14 μm long. For technological compatibility reasons, the gate insulator was manufactured as a composite of silicon oxide and nitride.

The measurements were performed on the especially designed measurement stand at WUT. The stand allows fully automated measurements of several transistor characteristics with various ion concentrations at different temperatures. The presented measurements were taken simultaneously for 10 ISFETs with the hydrogen ion concentration pH equal to 4, 7 and 10. Unfortunately, only 7 out of the 10 transistors mounted in the measurement unit were working properly. Consequently, all the defective transistors were not taken into account in the simulations. The output and transfer characteristics of the other 7 transistor measured at the pH value equal to 7 are presented.

Additionally, the measured output characteristics obtained for different pH values averaged for all the sensors, except for the three defective ones and the one having much higher drain current.

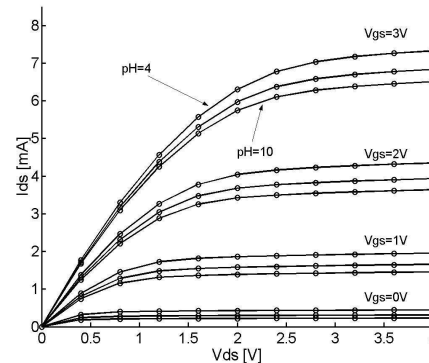
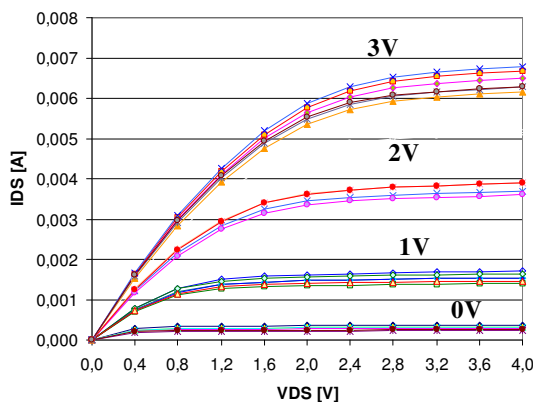


Figure 3.5. Output curves of sensors from IET (pH=7)

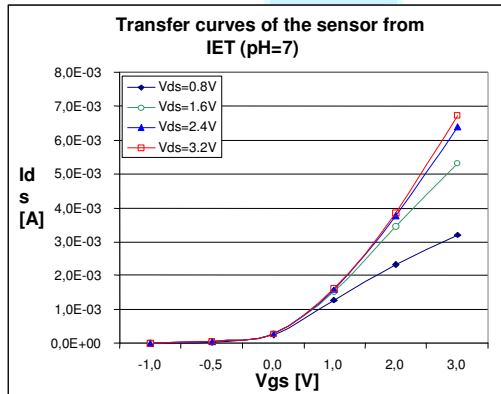


Figure 3.7. Transfer characteristics of the sensor from IET for the constant pH=7

Figure 3.6. Output curves of sensors from IET (for different pH)

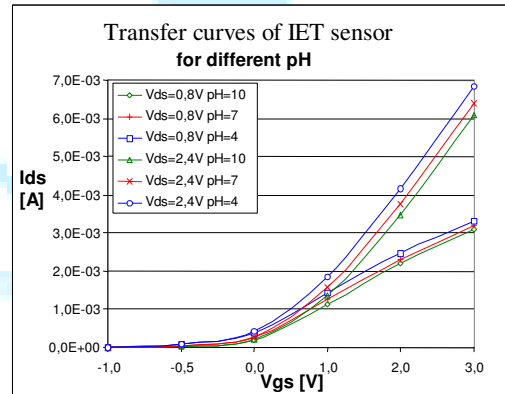


Figure 3.8. Transfer characteristics of the sensor from IET for different pH

The corresponding values of the threshold voltage extracted for the hydrogen ion concentration pH equal to 4, 7 and 10 were -528 mV, -368 mV, -245 mV respectively. This yields the gate surface potential shift of 160 mV between the pH values 4 and 7 and 123 mV between the pH values 7 and 10, whereas the expected theoretical value computed from the model should be in both cases equal to 159 mV. Thus, the average measured sensitivity for the acid solutions matches perfectly the theoretical one and amounts to 53 mV per decade of the ion concentration change. On the other hand, for the basic solutions the sensitivity drops down to only 41 mV per decade. This discrepancy could be explained by the not highest selectivity of the gate dielectric material. Then, bearing in mind that the pH values are the logarithmic function of hydrogen ion concentration, for low ion concentrations, the ISFET becomes more vulnerable to the presence of other ions than the hydrogen ones. These so-called disturbing ions bind with the active sites in the gate dielectric instead of the hydrogen ions hence degrading the ISFET sensitivity. This results in the appearance of a bending in the surface potential vs. pH characteristics, i.e. it becomes more flat for high pH values.

3.1.2 Model parameter extraction software

The parameter extraction was performed based on the presented above measurement results. For this purpose the extraction software were developed. It was implemented in MINUIT and MATLAB environments which offers a wide range of numerical methods for optimisation purposes. The idea of parameter extraction is the same for both of the tools. It consists of four separate steps. First, the initial guess of the set parameter is performed (with the range of acceptable changes). Secondly the device (ISFET) is simulated through model, after that the simulation results are compared with the measurements. If the fitting criterion is satisfied the parameters are stored, if not the parameters changed by the optimisation procedure are put to the model, procedure starts again.

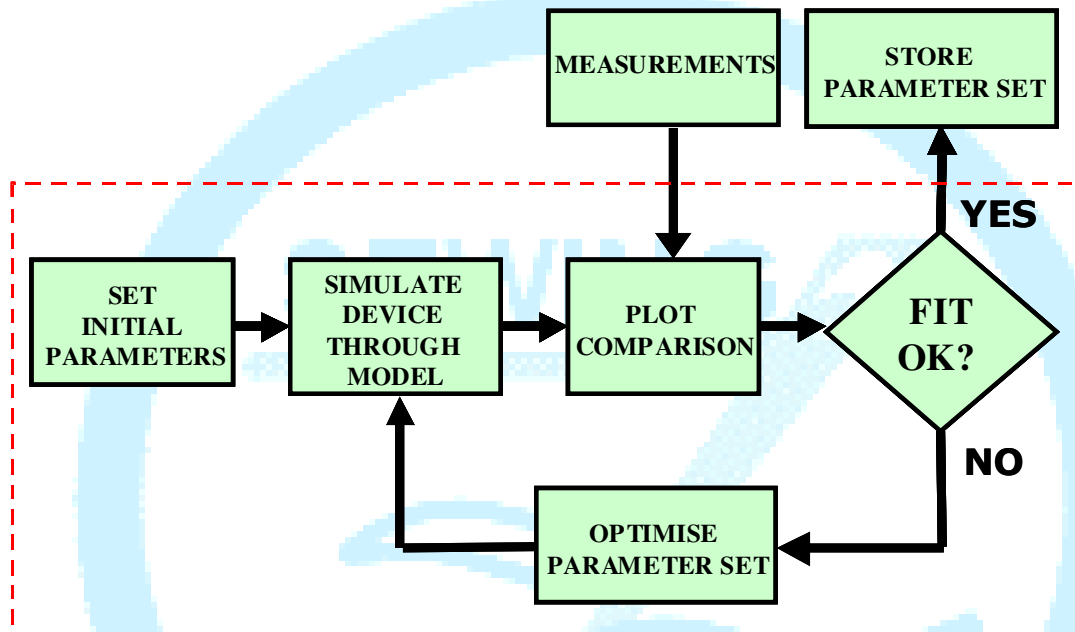


Figure 3.9. Extraction algorithm

3.1.3 Parameter extraction

The Shichman–Hodges model requires (besides the geometrical parameters W and L) 5 parameters to extract. These are: the threshold voltage V_T , the low electrical field carrier mobility μ_0 , the oxide capacitance C_{OX} (which can be roughly calculated knowing the geometrical dimensions and the dielectric constants of the gate oxide and ion sensitive oxide layer). The oxide capacitance was found to be equal to $4.54 \cdot 10^{-4} \text{ F/m}^2$.

Moreover, equations describing the carrier mobility contain two unknown quantities modifying the low electrical field mobility μ_0 : the mobility modulation coefficient Θ and the maximal carrier velocity v_{max} . Summarising, there are altogether seven ISFET model parameters, which are to be determined in the extraction procedure: the threshold voltage V_T , the mobility modulation coefficient Θ , the carrier mobility μ_0 , the maximal velocity v_{max} , C_{OX} – gate oxide capacitance and W, L .

In MATLAB the parameter extraction was performed employing a Newton-Gauss method based on the automatic procedure already implemented in this environment. The procedure uses the Least Mean Squares (LMS) optimisation criterion so as to find the optimal set of parameters.

In MINUIT the simplex method was used to determine the optimised value of the parameters after that the MIGRAD (implemented in MINUIT) package that incorporates a variety of gradient method was applied to find the best values of parameters.

In Figure 3.10–Figure 3.12 the parameter extraction results are presented according to sensor from IET. In Figure 3.10 the fitted output curves were presented with constant pH=7, in Figure 3.11 the fitted output curves for different pH were presented. The fitted transfer curves are demonstrated in Figure 3.12. As can be noticed, the fitting with usage of presented model gives reasonable, quite accurate results.

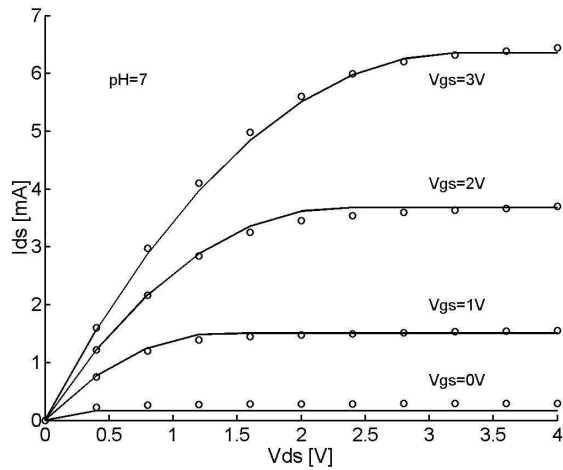


Figure 3.10. Fitted output curves of the IET sensor for constant pH=7

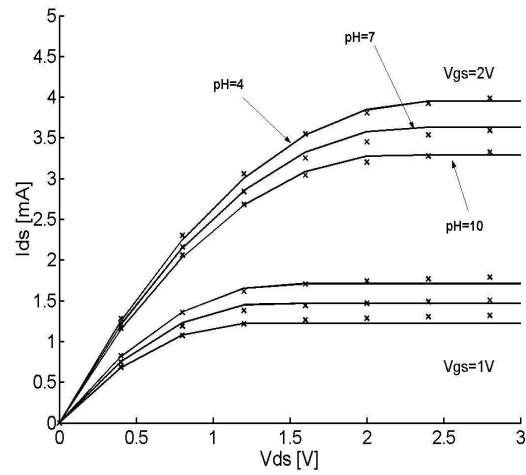


Figure 3.11. Fitted output curves of the IET sensor for various pH values

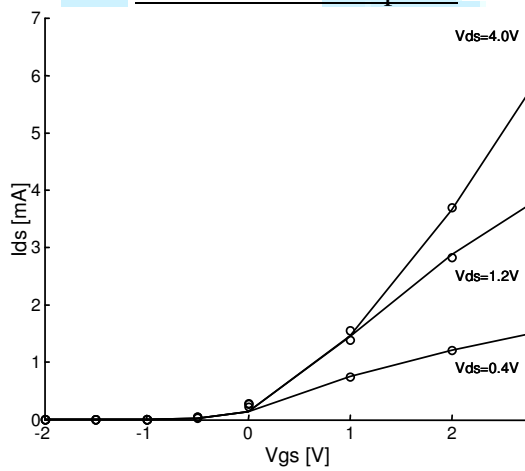


Figure 3.12. Fitted transfer curves of IET sensor for pH=7

Extracted parameters for sensor manufactured by IET are presented in Table 1.

Table 1 .Extracted parameters for ISFET from IET

TYPE	Parameter name	Values range	Staring value	Optimised value	Error [%]
SEMICONDUCTOR	W [μm]	635 – 640	638	638.113	4.24
	L [μm]	13 – 15	14	14.021	
	μ_0 [m^2/Vs]	0.06 – 0.11	0.091	0.097	
	C_{OX} [F/m^2]	$4.1\text{e-}4$ – $4.6\text{e-}4$	$4.504\text{e-}4$	$4.491\text{e-}4$	
	V_{TH} [V]	-1 – 0	-0.5998	-0.382	
	θ [1/V]	0.01 – 0.31	0.15	0.187	
	v_{MAX}	$0.8\text{e}5$ – $1.2\text{e}5$	$1.023\text{e}5$	$1.035\text{e}5$	
ELECTR OLYTE	pH_{PZC}	7 – 8	7.5	7.5	
	κ	0.6 – 1	0.85	0.87	
	γ	1 – 1.2	1.1	1.12	

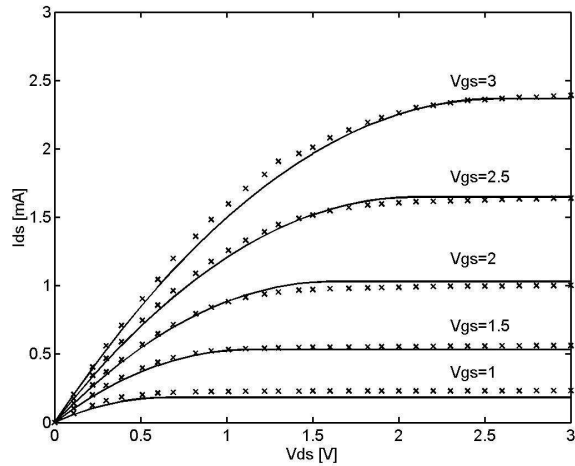


Figure 3.13. Fitted output curves of the LAAS sensor for constant pH=7

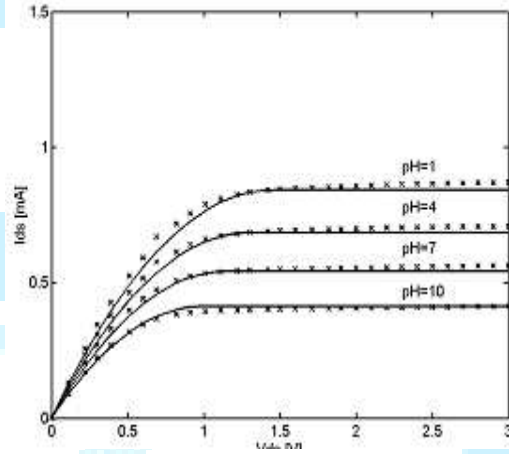


Figure 3.14. Fitted output curves of the LAAS sensor for various pH values

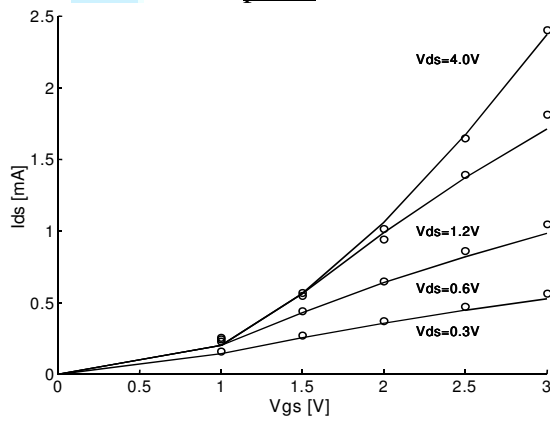


Figure 3.15. Measured and simulated transfer characteristics for pH=7.

Extracted parameters for the sensor from LAAS are presented in Table 2

Table 1. Extracted parameters for ISFET from LAAS

TYPE	Parameter name	Values range	Starting value	Optimised value	Error [%]
SEMICONDUCTOR	W [μm]	795 – 805	800	803.27	5.44
	L [μm]	28 – 32	30	30.9	
	μ_0 [m^2/Vs]	0.06 – 0.11	0.09	0.089	
	C_{OX} [F/m^2]	$4.0\text{e-}4$ – $5.5\text{e-}4$	$4.5\text{e-}4$	$4.108\text{e-}4$	
	V_{TH} [V]	0 – 0.7	0.5	0.376	
	θ [1/V]	0.01 – 0.31	0.15	0.128	
	v_{MAX}	$0.8\text{e}5$ – $1.2\text{e}5$	$1\text{e}5$	$1.071\text{e}5$	
ELECTROLYTE	pH_{PZC}	7 – 8	7.5	7.5	
	κ	0.6 – 1	0.85	0.885	
	γ	1 – 1.2	1.1	1.12	

As can be seen from the figures, the fitted curves for the improved model match very well the measured values, whereas such a good fit could not be attained when using the SPICE Level 1 model. The error in case of model Level 3 applied to the sensor from LAAS equals 4.24% whereas in IET case equals 5.44%. In case of LEVEL 1 the obtained error was seven times larger which proves that the proposed improvements to the model were justified.

3.2. CHEMFET model identification

3.2.1. Software for data storage and database management

For quick measurement of a large number of CHEMFET sensors, dedicated automatic equipment has been constructed. This equipment consists of a hydraulic system for automatic dosage of chemical compounds, a measuring head including sockets for a few sensors and programmable analogue-digital equipment for supplying sensors, measuring their currents and voltages. The set is controlled by the LabView PC-based application which generates XML data files [Report1]. For storing and quick access to the measured data a relational data base has been designed. At the moment it is arranged in the form of an MS ACCESS database operated from a MATLAB database controller application via the Database Toolbox. This controller application enables: a) importing XML measurement files and generation of SQL instructions, b) manual, automatic or mixed data filtering for elimination of noisy and faulty data, c) determination of chemical characteristics of sensors using filtered chemical-electrical measurements (transfer and output characteristics for different concentration levels of maximum 3 ions), d) identification of sensor model parameters by means of a MATLAB based special purpose characterisation tool, e) statistical analysis and visualisation of sensor parameters, f) storage of both the results of the data processing operations and also of processing algorithms (filtering, optimisation). Saving parameters of algorithms may enable tuning of data processing algorithms for maximum efficiency and accuracy.

3.2.2. Software for measured data visualisation and processing (LO)

During research on modelling CHEMFET sensors a number of software modules have been written for MATLAB environment, to support the following tasks:

- conversion of data between XML raw data format [Report1] and other binary, MATLAB-oriented formats [Report2] . M-files: `xml2mat`, `mat4opt`
- visualisation of raw data: `plot_session`
- visualisation of frequently used data subsets: `CHEMdisp`, `CHEMopdep`, `CHEMtdep`,...
- model analysis, characterisation and visualisation: see 3.2.3

The modules have been partially incorporated into the data management framework mentioned in 3.2.1.

3.2.3. Software for rough extraction of model parameters (JO,LO)

Model characterisation is optimisation based. Because of the very nature of nonlinear optimisation – good starting point (i.e. an approximation to model parameter vector) is needed to get efficiently in a neighbourhood of optimum. Thus a preliminary “rough characterisation” (“pre-extraction”) procedure has been developed to address specifically these needs. Pre-extraction procedure operates in two steps.

3.2.3.1. Nikolski-Eisenmann model

First, parameters of the chemical part of the CHEMFET model are approximated. For the Nikolski-Eisenmann model it is necessary to find sensor response, i.e. dependence of U_{RS} on activity of main ion a_m , for fixed and known activity a_s of an interfering ion.

$$U_{RS} + \frac{NV_T}{z_m} \ln(a_m + K_{m,s} a_s^{z_m/z_s}) = U_{GS} \approx const.$$

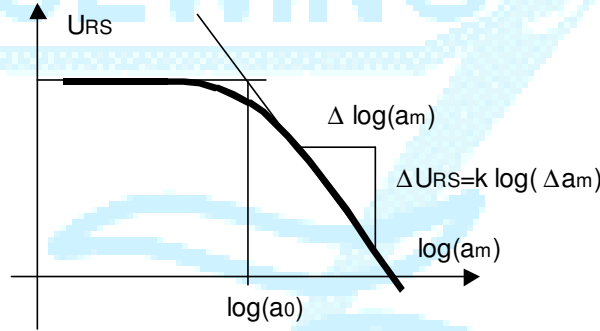


Figure 3.16. Illustration of calculations from the chemical response of a CHEMFET

From the plot in Fig. 3.16 we have: $a_0 = K_{m,s} a_s^{z_m/z_s}$ and maximum slope $k = \frac{NV_T}{z_m} \ln(10)$.

Knowing the temperature T , activities and electro-valencies of ions we can calculate N – the nonideality coefficient, and $K_{m,s}$ – the selectivity coefficient.

3.2.3.2. Nikolski and super-Nikolski models with identical valency of ions

For the Super-Nikolski model extraction procedure has been developed for the case of identical ions electrovalency. Since this extraction is only rough, this algorithm can be used also in the non-identical electrovalency case.

Let the sensor response be described by a basic model in ions concentration domain:

$$E_{GS} = E_{offs} - \psi_0 \ln(e_{GS}), \quad e_{GS} = c_{C1} + \sum_{j=2}^m K_j c_{Cj}, \quad E_{offs} = E_{FET} + \psi_0 \ln c_{1R}. \quad \text{Rough identification}$$

procedure consists of the following stages:

a) Nonideality index identification from a slope of $E_{GS}(c_{C1})$ in the linear, medium concentration region: $E^1 = E_{GS}(c_{C1}^1)$, $E^2 = E_{GS}(c_{C1}^2)$ are selected, $\psi_0 = (E^2 - E^1) / \ln(c_{C1}^1 / c_{C1}^2)$ is calculated and $n_i = kT/q\psi_0$ is obtained.

b) Offset voltage identification from a point $E^1 = E_{GS}(c_{C1}^1)$ in the linear region. We obtain: $E_{offs} = E^1 + \psi_0 \ln c_{C1}^1$ and then $E_{FET} = E_{offs} - \psi_0 \ln c_{1R}$.

c) Association constants. If not all K_{aj} are identical they influence the sensor response. On the slope characteristic $de_{GS}/dc_{C1} = d \exp[(-E_{GS} + E_{offs})/\psi_0] / dc_{C1}$ we can two plateau, left and right, in the small concentration region, dependent on association constants K_{a1} , K_{a2} . A ratio

of plateau: $r = e'_{GS \text{ left}} / e'_{GS \text{ right}}$ can be expressed by the formulae: $r = \frac{\left[\kappa_2 + \frac{\lambda(\kappa_1^2 - \kappa_2^2)/2}{(\kappa_2 + 1)/\lambda - 1} \right]}{\kappa_1}$, where

$\kappa_1 = \lambda(1 + \sqrt{1 + 4\bar{a}_{Ytot}K_{a1}}) - 1$, $\lambda = \frac{\bar{a}_{Lot}}{2\bar{a}_{Ytot}}$, $\kappa_2 = \lambda(1 + \sqrt{1 + 4\bar{a}_{Ytot}K_{a2}}) - 1$. If r is estimated from a

slope of the measured characteristic and K_{a2} is assumed then κ_1 and hence K_{a1} can be calculated.

d) Interfering ions contribution $w = \sum_{j=2,m} K_j c_{Cj}$ can be estimated from two points chosen on the

low concentration knee where the curvature is highest: $E^1 = E_{GS}(c_{C1}^1)$, $E^2 = E_{GS}(c_{C1}^2)$. We calculate $w = (c_{C1}^1 - \varepsilon c_{C1}^2) / (\varepsilon - 1)$ where $\varepsilon = \exp((E^2 - E^1) / \psi_0)$. If we have one type of interfering ions, then selectivity can be estimated from $K_j = w / c_{Cj}$. The intrinsic selectivity mentioned in (13) has to be recalculated from $K_j \kappa_1 / \kappa_2$.

The above rules of chemical response identification provide quite good accuracy. In the example shown in Fig 3.17 maximum fitting error was about 5 %.

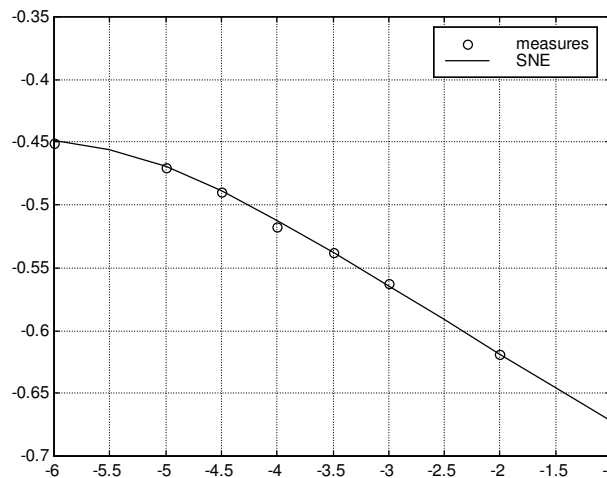


Figure 3.17. Chemical model response roughly fitted to measured points (V vs pK)

3.2.3.3. Rough extraction of the FET model

In the second step parameters of the FET model have to be estimated. It is advisable to have electrical characteristics of the CHEMFET for fixed ionic content of the electrolyte under test.

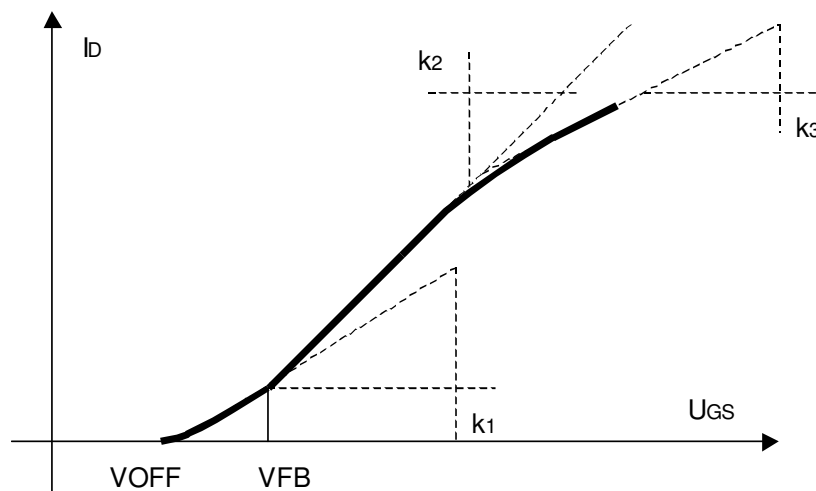


Figure 3.18. Illustration of calculations from a transfer I-V curve of a CHEMFET

From the transfer characteristics for small U_{DS} (linear region of operation) one can estimate the pinchoff voltage $VOFF$, the flat band voltage VFB , BETA and THETA parameters as sketched in the Fig.3.18.

For small U_{DS} (i.e. when $U_{DS}^2 \ll U_{DS}$) and for $U_{GS} < VFB$, $I_D \approx \beta(U_{GS} - VOFF)U_{DS}$, thus $k_1 \approx \beta \cdot U_{DS}$ and so β can be estimated.

For $U_{GS} < VFB$, $I_D \approx \beta[(U_{GS} - VOFF) + (r_0 - 1)(U_{GS} - VFB)] \cdot U_{DS}$, thus $k_2 \approx \beta \cdot r_0 \cdot U_{DS} = r_0 \cdot k_1$, and so r_0 can be found. For yet larger U_{GS} ,

$$I_D \approx \beta \left[(U_{GS} - VOFF) + \left(\frac{r_0}{1 + \theta(U_{GS} - VFB)} - 1 \right) (U_{GS} - VFB) \right] \cdot U_{DS}. \quad \text{Thus}$$

$$k_3 \approx \frac{\partial I_D}{\partial U_{GS}} = \beta \cdot U_{DS} \cdot \left[1 - r_0 + r_0 \frac{\theta \cdot VFB}{(1 + \theta \cdot (U_{GS} - VFB))^2} \right] \approx k_1 (1 - r_0 \cdot \theta \cdot VFB) \text{ and so } \theta \text{ parameter can be estimated.}$$

δ parameter can be approximated for linear mode of operation and larger U_{DS} values, when $I_D \approx \beta(U_{GS} - VOFF - U_{DS} \frac{1 + \delta}{2})U_{DS}$. Then $\frac{\partial I_D}{\partial U_{DS}} \approx \beta \cdot [(U_{GS} - VOFF) - (1 + \delta) \cdot U_{DS}]$.

The Early voltage VE can be found for saturation region of operation from the output conductance. Eg. assuming $VDSS1 \ll VE$ we have $\frac{\partial I_D}{\partial U_{DS}} \approx \frac{I_{DSS1}}{V_E}$. In geometric terms VE can be found as shown in Fig. 3.19.

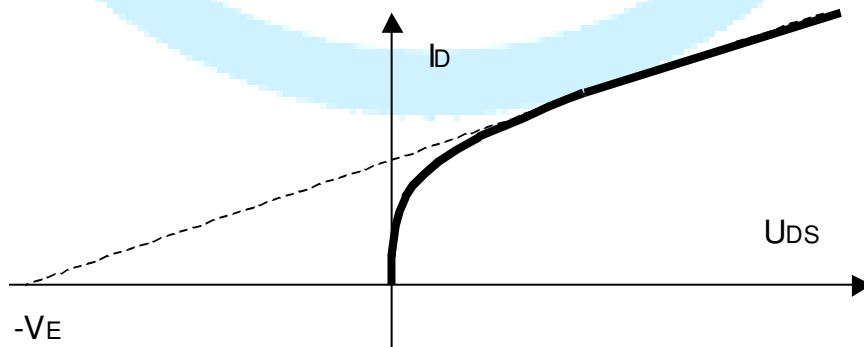


Figure 3.19. Illustration of the Early voltage estimation from the output I-V curve of a CHEMFET

3.2.4. Optimization based parameters extraction

For the optimization two approaches have been used. First was a mini-max formulation, that is the optimizer finds values of model parameters so that maximum relative error between measurement and model predicted data is the least. The objective function (to be minimized) took the following form

$$F(x) = \sum_j \frac{|y_j - y_j(x)|}{\max(|y_j|, \underline{y})}, \text{ where } y_j \text{ are measured values, } y_j(x) \text{ - corresponding responses}$$

of the model for given vector x or model parameters, and \underline{y} - a small positive number.

It has turned out that no constraints to the optimisation problem is needed, but linear scaling of variables was used, to make optimisation variables of the same order of magnitude, even though model variables are of different magnitude and physical meaning.

Another approach consisted of least squares minimization in the secondary parameters space \mathbf{x} . A dedicated software has been prepared in Matlab environment to minimize a sum of squared differences between modelled and measured CHEMFET responses, i.e. the objective function takes the form

$$F = \sum (y_j - y_j(\mathbf{x}))^2$$

where for the fixed URS measures $y_j(\mathbf{x}) = I_D(\mathbf{x}, U_{DSj}, U_{RSj}, T_j, \mathbf{a}_j)$ while for fixed current measures $y_j = U_{RS}(\mathbf{x}, I_{Dj}, U_{DSj}, T_j, \mathbf{a}_j)$ are taken into account. To improve numerical properties of the above minimization task scaling and box limiting of optimization parameters \mathbf{x} can be used.

3.2.5. Variability of sensor responses

Due to experimental nature of the CHEMFET devices that have been available to us so far – the information on variability should be treated as very preliminary. The plots below illustrate characteristics of 5 NO_3 sensors denoted with d01, ..., d05 (instances SE-06_no3-pc-1_001_1 through SE-06_no3-pc-1_001_5, according to our measurement lab notation).

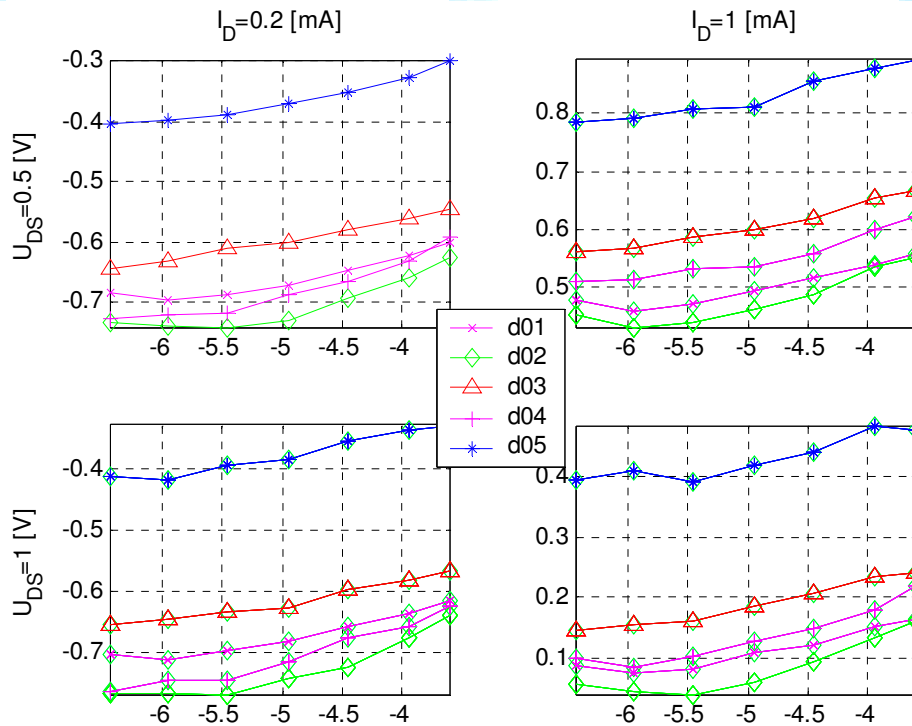


Figure 3.20. Illustration of sensor variability: chemical responses of 5 NO_3 CHEMFET sensors at different operating points.

The variability of the sensors which responses are shown in Fig.3.20 is substantial. Most of the variability can be compensated by one-point calibration that would offset vertical shift of the responses. For precise measurements such a calibration is not sufficient, since these particular sensors differ also significantly in selectivity coefficients – which is demonstrated by differences in slope of responses for low ionic activity. The final grade sensor have not been available to use at the time of this report writing, so no improvement of variability due to technological improvements can be reported yet.

Bibliography

- [ICSES02-LJO] L.J. Opalski, „Electro-chemical modeling of CHEMFET sensors”, Proc. ICSES’02, Świeradów-Zdrój, Poland, 2002.
- [ISESS03] A. Filipkowski, Andrzej Goralski, Jan Ogrodzki, Leszek Opalski, „Software for the system of European water monitoring”,...
- [MIXDES02-LJO] L.J. Opalski, Z. Gniewiński, W. Wróblewski, “On dependence of CHEMFET sensor response on operating point”, Proc. MIXDES’02, Wrocław, 2002.
- [MIXDES03-LJO] L.J. Opalski, „On modelling temperature dependence of CHEMFET response curves”, Proc. MIXDES’03, Łódź, 2003.
- [ECCTD03] J. Ogrodzki, L. Opalski, K. Zamłyński, „Modeling of CHEMFET sensors in SPICE”, Proc. ECCTD’03, Kraków, Poland, Sept. 2003.
- [Report1] L.J. Opalski, “Sensor measurement data format”, ISE, ver. 1.3 of 9.III.2003
- [Report2] L.J. Opalski, “Sensor measurement data visualisation in MATLAB”, ISE, 9.III.2003